

Parton distributions: a study of the new HERA data, α_s , the gluon and $p\bar{p}$ jet production

A. D. Martin^a, R. G. Roberts^b and W. J. Stirling^{a,c}

^a *Department of Physics, University of Durham, Durham, DH1 3LE*

^b *Rutherford Appleton Laboratory, Chilton, Didcot, Oxon, OX11 0QX*

^c *Department of Mathematical Sciences, University of Durham, Durham, DH1 3LE*

Abstract

New data, especially HERA measurements of the proton structure function at small x , allow the opportunity to improve our knowledge of the gluon and quark distribution functions. We perform a global analysis which incorporates these new precise data, and which extends down to $Q^2 = 1.5 \text{ GeV}^2$. We discuss the sensitivity to the value of α_s and the improvement in the determination of the gluon. We compare the predictions of the single jet inclusive cross section with recent measurements from the Fermilab Tevatron.

Predictions for hard scattering processes involving hadrons rely on a precise knowledge of the parton distribution functions. Traditionally these are determined from global analyses of data for a wide range of processes, see for example [1, 2]. As the precision of data improves and the kinematic domain of the measurements enlarges we obtain a more rigorous test of perturbative QCD and a better knowledge of the parton distributions. This is well illustrated by the new measurements [3, 4] of the proton structure function at HERA, which are more precise and extend to lower x than hitherto.

The significant improvement in the data demands a concomitant refinement of the parton distributions. In this Letter we describe a new global analysis, based on next-to-leading-order DGLAP evolution, of the type described in Ref. [1] but with the following special features:

- (i) structure function data down to $Q^2 = 1.5 \text{ GeV}^2$ are included;
- (ii) fits are performed for two different values of the QCD coupling, the standard “deep inelastic scattering” value ($\alpha_s(M_Z^2) = 0.113$) [5] and a larger value ($\alpha_s(M_Z^2) = 0.120$) suggested, for example, by measurements at LEP [6];
- (iii) particular attention is paid to the small x behaviour of the gluon and sea quark distributions;
- (iv) the single jet inclusive cross section is predicted and compared with the new CDF [7] and D0 [8] measurements at the Fermilab $p\bar{p}$ collider.

We elaborate on these aspects of the analysis in turn below.

In previous analyses we fitted to structure function data with $Q^2 > 5 \text{ GeV}^2$.¹ However the “dynamical” partons of the GRV model [9] were found to give a good description of data down to $Q^2 \sim 1 \text{ GeV}^2$, although the new HERA measurements [3, 4] at low Q^2 do show some systematic discrepancy between the GRV predictions and the data. In this respect it is important to investigate whether this signals a problem for DGLAP evolution at such low scales or for the assumptions implicit in the dynamical parton model. We therefore include all data with $Q^2 \geq 1.5 \text{ GeV}^2$. The choice $\alpha_s(M_Z^2) = 0.113$ corresponds to the optimum QCD coupling as determined by the scaling violations of the fixed-target deep inelastic data. The key data here are the BCDMS $F_2^{\mu p, d}$ measurements [10] in the interval $0.3 \lesssim x \lesssim 0.5$. There is, however, some indication that the HERA structure function data and the Fermilab jet data prefer a larger value of the coupling [11, 12, 13, 14]. To illustrate this point we therefore also present results of a second global fit in which the coupling is fixed at $\alpha_s(M_Z^2) = 0.120$. We call the resulting set of partons² R_1 and R_2 respectively.

¹Contamination by higher-twist contributions at large x is avoided by the additional cut $W^2 = Q^2(1-x)/x > 10 \text{ GeV}^2$.

²These new distributions were presented in preliminary form at the Rome DIS96 Workshop.

The advent of the HERA measurements of F_2 has considerably improved our knowledge of the gluon and sea quark distributions in the small x regime. We may represent their leading small x behaviour by the forms

$$xg \rightarrow x^{-\lambda_g(Q^2)}, \quad xS \rightarrow x^{-\lambda_S(Q^2)}. \quad (1)$$

In the perturbative region the evolution of the sea quark distributions is driven by the gluon, which is the dominant parton at small x , via the $g \rightarrow q\bar{q}$ splitting. The distributions are therefore correlated at small x , and for this reason most previous global analyses set $\lambda_S = \lambda_g$ in (1) at the input scale, usually taken to be $Q_0^2 = 4 \text{ GeV}^2$. Even disregarding non-perturbative effects, this expectation is only approximate. As we evolve up in Q^2 using the DGLAP evolution equations, $\partial g/\partial \ln Q^2 = P_{gg} \otimes g + \dots$ and $\partial q/\partial \ln Q^2 = P_{qg} \otimes g + \dots$, the effective exponents $\lambda_i(Q^2)$ increase with Q^2 , and satisfy

$$\lambda_S(Q^2) = \lambda_g(Q^2) - \epsilon, \quad (2)$$

where ϵ is positive and slowly varying with Q^2 , provided that the evolution is sufficiently long. Typically we find $\epsilon \sim 0.05$ at $Q^2 \sim 200 \text{ GeV}^2$, see below. That is, DGLAP evolution leads to a sea distribution which is slightly less steep in x than the gluon distribution.

The precision of the new HERA small x structure function data is now such that we can begin to study the small x behaviour of the quarks and gluons in detail. We therefore allow both λ_S and λ_g to be free parameters at the input scale, which we here take to be $Q_0^2 = 1 \text{ GeV}^2$. To see the extent to which λ_S and λ_g can be individually determined, we also perform fits with $\lambda_S = \lambda_g$ at Q_0^2 . Where appropriate, we show properties of these additional parton sets, which we label R_3 and R_4 corresponding to $\alpha_s(M_Z^2) = 0.113$ and 0.120 respectively.

Another interesting development is the constraint that the high statistics jet data from Fermilab are starting to impose on the partons and the QCD coupling α_s . The slope of the inclusive jet transverse energy (E_T) distribution is particularly sensitive to the value of α_s [11, 13]. In the region where the data are most definitive, $50 \lesssim E_T \lesssim 200 \text{ GeV}$, the jets arise from gluon-initiated QCD processes. Hence the data can give a tight constraint on $\alpha_s(\mu^2)g(x, \mu^2)$ where the gluon is sampled in the region $x \sim 2E_T/\sqrt{s} \sim 0.1$, but at a high scale $\mu^2 \sim E_T^2$ where evolution tends to wash out the differences between the parton sets. We compare the predictions based on our new R_1 and R_2 sets with CDF [7] and preliminary D0 [8] jet E_T distributions to demonstrate the potential discriminating power of the data.

As in our previous studies, we adopt the following simple analytic form for the starting distributions:³

$$xf_i(x, Q_0^2) = A_i x^{-\lambda_i} (1-x)^{\eta_i} (1 + \epsilon_i \sqrt{x} + \gamma_i x), \quad (3)$$

for $i = u_V, d_V, S, g$, but at the lower scale $Q_0^2 = 1 \text{ GeV}^2$. Here S represents the total sea quark distribution. At Q_0^2 , only the u, d, s distributions are non-zero, and so $S \equiv 2(\bar{u} + \bar{d} + \bar{s})$.

³The distributions are defined in the $\overline{\text{MS}}$ renormalization and factorization schemes.

The flavour structure of the sea is taken to be

$$\begin{aligned} 2\bar{u} &= 0.4S - \Delta \\ 2\bar{d} &= 0.4S + \Delta \\ 2\bar{s} &= 0.2S, \end{aligned} \tag{4}$$

with

$$x\Delta \equiv x(\bar{d} - \bar{u}) = A_{\Delta}x^{0.3}(1-x)^{n_S}(1+\gamma_{\Delta}x). \tag{5}$$

The suppression of the strange distribution is motivated by data on neutrino-induced deep inelastic dimuon production obtained by the CCFR collaboration [15]. In our previous studies this factor 2 suppression was applied at $Q_0^2 = 4 \text{ GeV}^2$, rather than at $Q_0^2 = 1 \text{ GeV}^2$ as in (4). The consequence is that the strange sea is slightly larger at $Q^2 = 4 \text{ GeV}^2$ and, in fact, in better agreement with the CCFR measurement. That is, the strange sea lies more centrally in the allowed band for $s(x, Q^2 = 4 \text{ GeV}^2)$, determined by the next-to-leading order CCFR analysis, than does the MRS(A) curve shown in Fig. 4 of Ref. [1]. The u, d flavour symmetry breaking distribution $\Delta(x)$ is chosen to give good agreement with the NMC measurement of the Gottfried sum [16], and the NA51 measurement of the Drell-Yan pp/pn asymmetry [17].

In previous analyses, we treated the charm quark as massless and evolved its distribution from zero at $Q^2 = m^2$, where $m^2 = 2.7 \text{ GeV}^2$ was chosen to reproduce the EMC charm data [18]. Now that we have lowered the starting scale to $Q_0^2 = 1 \text{ GeV}^2$ it is necessary to smooth out the onset of charm. We take $c(x, Q_0^2) = 0$ and evolve up in Q^2 with four flavours but since Q_0^2 is now much lower, this unmodified density would overestimate the observed $F_2^c(x, Q^2)$. We simply suppress the generated charm density by a smooth factor [19] which mimics the threshold behaviour of the massive quark, i.e.

$$c(x, Q^2) \longrightarrow \left\{ 1 - \mathcal{N}\left(\frac{m_0^2}{Q^2}\right) \right\} c(x, Q^2) \tag{6}$$

where

$$\mathcal{N}(z) = 6z \left[1 - \frac{2z}{\sqrt{1+4z}} \ln \left(\frac{\sqrt{4z+1}+1}{\sqrt{4z+1}-1} \right) \right] \tag{7}$$

with $m_0^2 = 3.5 \text{ GeV}^2$ chosen give a reasonable description of the EMC [18] and preliminary H1 [20] measurements of the charm structure function F_2^c . We see from Fig. 1 that this approximate treatment of charm does indeed give a satisfactory description of F_2^c at present, but as the data improve it will become necessary to give a more satisfactory treatment of charm-mass effects.

Using the above parton parametrizations at $Q_0^2 = 1 \text{ GeV}^2$ we perform global next-to-leading order DGLAP fits to the deep inelastic and related hard scattering data that were used in the MRS(A) analysis [1], but now including data down to $Q^2 = 1.5 \text{ GeV}^2$, supplemented by SLAC [21], E665 [22] and updated NMC [23] structure function measurements and, most importantly, the new H1 [3] and ZEUS [4] F_2 data. We present the results of the four different fits $R_1 - R_4$, which we described above. The optimum values of the starting distribution parameters are

listed in Table 1. Note that three of the four A_i coefficients are determined by the momentum and flavour sum rules. The fourth (A_S) is a fitted parameter. Because of the different values of Q_0^2 , these parameters cannot be directly compared with the corresponding parameters from previous MRS analyses. The χ^2 values found in the four fits for the deep inelastic structure

		R ₁	R ₂	R ₃	R ₄
		$\lambda_S \neq \lambda_g$		$\lambda_S = \lambda_g$	
	$\alpha_s(M_Z^2)$	0.113	0.120	0.113	0.120
	$\Lambda_{\overline{\text{MS}}}^{n_f=4}$ (MeV)	241	344	241	344
Glue	(A_g)	24.4	14.4	2.07	0.746
	λ_g	-0.41	-0.51	0.04	0.04
	η_g	6.54	5.51	4.56	4.38
	ϵ_g	-4.64	-4.20	-3.05	-3.85
	γ_g	6.55	6.47	6.83	18.1
Valence	λ_u	0.60	0.61	0.59	0.66
	η_u	3.69	3.54	3.67	3.55
	ϵ_u	-1.18	-0.98	-1.02	-1.08
	γ_u	6.18	6.51	6.36	5.43
	λ_d	0.24	0.24	0.25	0.26
	η_d	4.43	4.21	4.45	4.18
	ϵ_d	5.63	7.37	4.82	9.64
	γ_d	25.5	29.9	23.5	26.3
Sea	A_S	0.42	0.37	0.92	0.92
	λ_S	0.14	0.15	0.04	0.04
	η_S	9.04	8.27	9.38	8.93
	ϵ_S	1.11	1.13	-1.65	-2.34
	γ_S	15.5	14.4	11.8	12.0
	A_Δ	.039	.036	.040	.038
	γ_Δ	64.9	64.9	64.9	64.9

Table 1: The numerical values of the starting distribution parameters of the four sets of partons. Note that A_g is fixed by the momentum sum rule, and is therefore not a free parameter.

function subsets of the data are listed in Table 2. We have not included the comparisons of each fit with other constraints such as prompt photon production, W^\pm asymmetry, di-lepton production, and Drell-Yan pp/pn asymmetry, but in every case the quality of the descriptions is close to that of MRS(A,A') [1, 24].

An idea of the quality of the description of the small x measurements of F_2^p that is obtained in the R₁ and R₂ fits can be seen from the compilation shown in Fig. 2. For comparison we also

Experiment	# data	χ^2			
		R ₁	R ₂	R ₃	R ₄
H1 F_2^{ep}	193	158	149	200	171
ZEUS F_2^{ep}	204	326	308	378	329
BCDMS $F_2^{\mu p}$	174	265	320	247	311
NMC $F_2^{\mu p}$	129	155	147	151	152
NMC $F_2^{\mu d}$	129	139	129	133	132
NMC $F_2^{\mu n}/F_2^{\mu p}$	85	136	132	136	133
E665 $F_2^{\mu p}$	53	8	8	8	8
SLAC F_2^{ep}	70	108	95	104	96
CCFR $F_2^{\nu N}$	66	41	56	42	52
CCFR $xF_3^{\nu N}$	66	51	47	50	44
CDF $d\sigma/dE_T$					
50 < E_T < 200 GeV	24	222	52	169	93
E_T > 200 GeV	11	10	20	9	7
D0 $d\sigma/dE_T$					
50 < E_T < 200 GeV	14	103	72	50	126
E_T > 200 GeV	12	26	22	12	41

Table 2: χ^2 values for some of the data used in the global fit. The $d\sigma/dE_T$ jet data are predicted, not fitted.

show the prediction of the GRV set of (“dynamical”) partons [9]. In the GRV analysis charm is treated as a heavy quark (rather than as a parton), this contribution being included in the GRV curves shown.

Fig. 3 displays the Q^2 dependence of the exponents λ_g and λ_S of the $x^{-\lambda}$ behaviour of the gluon and sea quark distributions, see Eq. (1). To be precise the curves are obtained by assuming that the parton forms (3) describe the evolved distributions at any Q^2 and then determining the $\lambda_i(Q^2)$ by a five-parameter $(A_i, \lambda_i, \eta_i, \epsilon_i, \gamma_i)$ fit to $xg(x, Q^2)$ and $xS(x, Q^2)$ at each Q^2 . The upper plot is obtained from the R₂ set of partons, which have $\lambda_S \neq \lambda_g$ at $Q_0^2 = 1 \text{ GeV}^2$. It shows that the gluon is valence-like at the input scale. However evolution in Q^2 rapidly steepens the small x shape of the gluon and by $Q^2 \sim 2 \text{ GeV}^2$ it is already starting to drive the sea quark distribution, leading to the DGLAP expectation shown in Eq. (2). It is interesting to note that the cross-over point, $\lambda_g = \lambda_S$, occurs in the region $Q^2 \sim 5 \text{ GeV}^2$. Thus the behaviour is approximately compatible with the MRS(A,A’) sets of partons which were required to have $\lambda_g = \lambda_S$ at the $Q_0^2 = 4 \text{ GeV}^2$ starting scale. The data points shown in Fig. 3 are obtained by the H1 collaboration [3] by fitting their measurements of F_2^p for $x < 0.1$ in the regions appropriate to each Q^2 bin by the form $x^{-\lambda}$. Due to the simplified form of the H1 parametrization and the extensive x range of the data fitted (which drifts to larger x as Q^2

increases), strictly speaking these values should not be compared with λ_S . Nevertheless they do give a good representation of the errors as a function of Q^2 .

We saw in Table 2 that the χ^2 values for the $R_{2,4}$ descriptions of the BCDMS $F_2^{\mu p}$ data are significantly worse than those for $R_{1,3}$. The reason, as already mentioned, is that it is these data that constrain $\alpha_s(M_Z^2)$ to be 0.113 in the global fit. The sets with $\alpha_s(M_Z^2) = 0.120$ lead to scaling violations for the structure function which are stronger than those measured by BCDMS. This is illustrated in Fig. 4, which compares the R_1 and R_2 descriptions of the “medium x ” SLAC [21] and BCDMS [10] proton structure function measurements. Only those data points which pass the $W^2 > 10 \text{ GeV}^2$ cut (and which are therefore included in the global fit) are shown. The value of α_s is mainly constrained by the BCDMS data (on both hydrogen and deuterium targets) in the $x = 0.35, 0.45$ bins. Here the preference of the data for the R_1 set is evident. Although the SLAC data have a slight preference overall for the larger α_s value (see Table 2), the error bars are larger and so the statistical significance is weaker. There is also the possibility that the lower Q^2 data are contaminated with higher-twist contributions, which would of course distort the α_s measurement. However, a careful analysis [5] of the combined SLAC and BCDMS data, incorporating a phenomenological higher-twist contribution, yields the value

$$\alpha_s(M_Z^2) = 0.113 \pm 0.005, \quad (8)$$

where the statistical and systematic errors have been combined.

The NLO QCD fits to the medium/large x fixed-target structure function data are relatively insensitive to the gluon distribution which, in the MRS global fits, is constrained in this x region by the large p_T prompt photon data, see for example Ref. [24]. However at small x there is a significant $\alpha_s -$ gluon correlation, since $\partial F_2 / \partial \ln Q^2 \sim \alpha_s P^{qg} \otimes g$. This is evident in Fig. 5(a), which shows the gluon distributions of the four R fits in the small x HERA region at $Q^2 = 5 \text{ GeV}^2$. At small x the R_1 gluon is evidently some 10 – 20% larger than the R_2 gluon. The same hierarchy is visible in the R_3 and R_4 gluons, but these are both slightly steeper. The reason is that constraining λ_g to be equal to λ_S forces a larger value for the former, see Fig. 3, and a correspondingly steeper gluon. Given that the HERA data clearly favour *different* values for λ_g and λ_S (Table 2) we may take the spread in the R_1, R_2 gluons to represent the uncertainty in the distribution at small x . It is interesting to note that the previous MRS(A') gluon lies within this band.

Also shown in Fig. 5(a) is the GRV “dynamical” gluon [9]. This is much larger than any of the four R gluons, and therefore yields a more rapid Q^2 evolution for the structure function. This was already evident in Fig. 2, which also showed that such a strong Q^2 dependence is now ruled out by the H1 and ZEUS data.

Figure 5(b) shows the relative behaviour of the four R gluons at $Q^2 = 10^4 \text{ GeV}^2$, the scale relevant for the Fermilab jet data. As expected, the curves have evolved closer together, although the qualitative differences seen at $Q^2 = 5 \text{ GeV}^2$ are still apparent. Quantitatively, we see that the crossover points of the R_1 and R_3 gluons (with the same α_s) have moved to smaller

x in accordance with the evolution equation, $\partial g/\partial \ln Q^2 \sim P_{gg} \otimes g$, where g is sampled in the convolution at slightly larger x .

Figure 6 compares the NLO QCD predictions⁴ for the single jet inclusive E_T distribution at the Tevatron, using the new R_1 and R_2 sets, with data from the CDF [7] and D0 [8] collaborations. Only the statistical errors on the data are shown, and in each case the data have been renormalized by a constant factor to give the best overall fit.⁵ As the perturbative QCD predictions become unstable at small E_T , only data with $E_T > 50$ GeV are included in the comparison. The corresponding χ^2 values are listed in Table 2. The first and most obvious point to note is that highest E_T CDF points tend to lie above the theoretical prediction, a tendency which is *not* evident in the D0 data. The “disagreement” with the CDF data has been the subject of much recent discussion, explanations ranging over a variety of new physics effects [26] (but see also [14, 27, 28]). In view of the fact that the large E_T D0 data appear perfectly compatible with the $R_{1,2}$ predictions, we believe that it is premature to draw any firm conclusions about disagreements with perturbative QCD. More interesting is the discriminating power of the high-precision $E_T \lesssim 200$ GeV jet data. Since the Q^2 evolution length is so long, the steepness of the parton distributions in x , and therefore of the jet E_T distribution, is strongly correlated with the value of α_s [11]. The effect is clearly seen in the differences between the R_1 ($\alpha_s(M_Z^2) = 0.113$) and R_2 ($\alpha_s(M_Z^2) = 0.120$) predictions in Fig. 6. One could therefore, at least in principle, use these data to measure α_s , see for example Ref. [13]. Such an analysis would however require a careful consideration of the systematic errors on the *shape* of the measured E_T distribution, and also of the correlation with the gluon distribution, which is responsible for a significant fraction of the uncertainty in the cross section in this E_T range. For instance, if we consider the R_1 and R_3 descriptions (which have the same α_s) of the medium- E_T CDF jet data, the reduction in χ^2 from 222 to 169 in Table 2 is due primarily to the difference in slope of the gluons in the $x \sim 0.1 - 0.2$ region, as shown in Fig. 5(b). However the slope of the jet cross section is more sensitive to α_s than to the change in the gluon distribution, as reflected in the reduction of χ^2 to 52 for these jet data for parton set R_2 .

Taken at face value, the CDF and D0 jet data would appear to favour a larger value of α_s , of order 0.122 and 0.118 respectively. This suggests that a global analysis incorporating these data would yield a set of partons very similar to R_2 with $\alpha_s(M_Z^2) \approx 0.120$.

In conclusion, we are able to obtain an excellent and economical NLO DGLAP-based description of a wide range of deep inelastic and hard scattering data over an increasingly large kinematic domain, namely down to $Q^2 = 1.5$ GeV² and $x \sim 10^{-4}$. The new HERA data have considerably improved our knowledge of the gluon in the small x region. We present⁶ two sets of partons R_1 and R_2 corresponding to two values of α_s , respectively $\alpha_s(M_Z^2) = 0.113$ (the “classic”

⁴The calculation uses the next-to-leading-order parton level Monte Carlo JETRAD [25] and the cuts and jet algorithm applied directly to the partons are modelled as closely as possible to the experimental set-up. We thank Nigel Glover for help in performing these calculations.

⁵Note that the normalization factors shown in Fig. 6 are in each case well within the quoted experimental uncertainty.

⁶The FORTRAN code for the R sets is available by electronic mail from W.J.Stirling@durham.ac.uk

DIS value determined by the scaling violations of the fixed-target data), and $\alpha_s(M_Z^2) = 0.120$ (favoured by the HERA F_2 and Fermilab jet data). It is clear that including the jet data, with statistical errors only, in the global analysis would in fact discriminate between our two sets⁷ of partons in favour of R_2 .

Acknowledgements

We thank Jerry Blazey, Albert De Roeck, Nigel Glover, Al Goshaw, Mark Lancaster, Robert Thorne, Wu-Ki Tung and Andreas Vogt for useful discussions.

References

- [1] A.D. Martin, R.G. Roberts and W.J. Stirling, Phys. Rev. **D50** (1994) 6734.
- [2] CTEQ collaboration: J. Botts *et al.*, Phys. Lett. **B304** (1993) 159; H.L. Lai *et al.*, Phys. Rev. **D51** (1995) 4763.
- [3] H1 collaboration: preprint DESY 96-039 (1996), to be published in Zeit. Phys.
- [4] ZEUS collaboration: M. Derrick *et al.*, Zeit. Phys. **C69** (1996) 607; preprint DESY 96-076 (1996), to be published in Zeit. Phys.
- [5] A. Milsztajn and M. Virchaux, Phys. Lett. **B274** (1992) 221.
- [6] S. Bethke, in Proc. QCD94 Conference, Montpellier, July 1994, Nucl. Phys. **B** (Proc. Suppl.) **39BC** (1995) 198.
- [7] CDF collaboration: F. Abe *et al.*, preprint Fermilab-PUB-96/020-E (1996).
- [8] D0 collaboration: J. Blazey, presented at the XXXI Rencontres de Moriond, QCD and High Energy Hadronic Interactions, March 1996.
- [9] M. Glück, E. Reya and A. Vogt, Zeit. Phys. **C67** (1995) 433.
- [10] BCDMS collaboration: A.C. Benvenuti *et al.*, Phys. Lett. **B223** (1989) 485.
- [11] A.D. Martin, R.G. Roberts and W.J. Stirling, Phys. Lett. **B356** (1995) 89.
- [12] R.D. Ball and S. Forte, Phys. Lett. **B358** (1995) 365.
- [13] W.T. Giele, E.W.N. Glover and J. Yu, Phys. Rev. **D53** (1996) 120.

⁷The two sets R_3 and R_4 with $\lambda_S = \lambda_g$ at $Q_0^2 = 1 \text{ GeV}^2$ are disfavoured by the HERA data and are used only for comparison.

- [14] E.W.N. Glover, A.D. Martin, R.G. Roberts and W.J. Stirling, University of Durham preprint DTP/96/22 (1996), to be published in Phys. Lett.
- [15] CCFR collaboration: A.O. Bazarko *et al.*, Zeit. Phys. **C65** (1995) 189.
- [16] NMC: P. Amaudruz *et al.*, Phys. Rev. Lett. **66** (1991) 2712.
- [17] NA51 collaboration: A. Baldit *et al.*, Phys. Lett. **B332** (1994) 244.
- [18] EMC collaboration: J.J. Aubert *et al.*, Nucl. Phys. **B213** (1983) 31.
- [19] H. Georgi and H.D. Politzer, Phys. Rev. **D14** (1976) 1829.
- [20] H1 collaboration: A. De Roeck, 2nd Epiphany Conf., Krakow, January 1996; K. Daum, DIS96 Workshop, Rome, April 1996.
- [21] L.W. Whitlow *et al.*, Phys. Lett. **B282** (1992) 475.
L.W. Whitlow, preprint SLAC-357 (1990).
- [22] E665 collaboration: M.R. Adams *et al.*, preprint Fermilab-PUB-95/396-E (1996).
- [23] NMC collaboration: M. Arneodo *et al.*, preprint CERN-PPE/95-138 (1995).
- [24] A.D. Martin, R. G. Roberts and W.J. Stirling, Phys. Lett. **B354** (1995) 155.
- [25] W.T. Giele, E.W.N. Glover and D.A. Kosower, Phys. Rev. Lett. **73** (1994) 2019.
- [26] V. Barger, M.S. Berger and R.J.N. Phillips, Madison preprint MADPH-95-920 (1995).
G. Altarelli, N. Di Bartolomeo, F. Feruglio, R. Gatto and M. Mangano, CERN preprint CERN-TH/96-20 (1996).
P. Chiappetta, J. Layssac, F.M. Renard and C. Verzegnassi, Marseille preprint CPT-96-P-3304 (1996).
M. Bander, UC Irvine preprint UCI-TR-96-7 (1996).
R.S. Chivukula, A.G. Cohen and E.H. Simmons, Boston University preprint BUHEP-96-5 (1996).
J. Ellis and D.A. Ross, preprint CERN-TH/96-108 (1996).
- [27] CTEQ collaboration: J. Huston *et al.*, Michigan State preprint MSU-HEP-50812 (1995);
H.L. Lai and W.-K. Tung, Michigan State preprint MSU-HEP-60508 (1996).
- [28] M. Klasen and G. Kramer, preprint DESY 96-077 (1996).

Figure Captions

- Fig. 1 The description of the EMC [18] and preliminary H1 [20] data for $F_2^c(x, Q^2)$ by the R_1 set of partons. The other R_i sets of partons give essentially identical values of F_2^c .
- Fig. 2 The continuous and dashed curves correspond to the values of the proton structure function F_2 obtained from the R_1 and R_2 sets of partons (which have, respectively, QCD couplings corresponding to $\alpha_s(M_Z^2) = 0.113$ and 0.120) at twelve values of x chosen to be the most appropriate for the new HERA data. For display purposes we add $0.5(12 - i)$ to F_2 each time the value of x is decreased, where $i = 1, 12$. For comparison the dotted curves show the prediction obtained from the GRV set of partons [9]. The experimental data are assigned to the x value which is closest to the experimental x bin. Thus the ZEUS data [4] are shown in groupings with x values $(3.5, 6.3, 6.5 \times 10^{-5})$, $(1.02, 1.20 \times 10^{-4})$, $(1.98, 2.53 \times 10^{-4})$, $(4.0, 4.5 \times 10^{-4})$, $(6.32, 8.00 \times 10^{-4})$, $(1.02, 1.20 \times 10^{-3})$, (1.612×10^{-3}) , $(2.53, 2.60 \times 10^{-3})$, (4.00×10^{-3}) , (6.325×10^{-3}) , (1.02×10^{-2}) , (1.612×10^{-2}) , and the H1 data [3] in groupings with x values $(3.2, 5.0 \times 10^{-5})$, $(0.80, 1.30 \times 10^{-4})$, $(2.0, 2.5 \times 10^{-4})$, (5.0×10^{-4}) , $(6.3, 8.0 \times 10^{-4})$, (1.3×10^{-3}) , (1.585×10^{-3}) , $(2.0, 2.5, 3.2 \times 10^{-3})$, $(3.98, 4.0, 5.0 \times 10^{-3})$, (6.3×10^{-3}) , (8.0×10^{-3}) , (1.3×10^{-2}) . The E665 data [22], which are shown on the curves with the five largest x values, are measured at $x = (2.46 \times 10^{-3})$, $(3.698, 5.2 \times 10^{-3})$, (6.934×10^{-3}) , (8.933×10^{-3}) , $(1.225, 1.73 \times 10^{-2})$.
- Fig. 3 The exponents λ_g and λ_S as a function of Q^2 calculated from the R_2 (upper plot) and R_4 (lower plot) sets of partons. Also shown are the values of λ obtained by the H1 collaboration [3] by fitting their data to the form $F_2 = Ax^{-\lambda}$ for $x < 0.1$ at different values of Q^2 .
- Fig. 4 The fit to the “medium” x SLAC [21] and BCDMS [10] data for F_2^p by the R_1 and R_2 sets of partons which have, respectively, QCD couplings corresponding to $\alpha_s(M_Z^2) = 0.113$ and 0.120 .
- Fig. 5 The gluon distribution at (a) $Q^2 = 5 \text{ GeV}^2$ (upper figure) and (b) 10^4 GeV^2 (lower figure). The bold curves correspond to the new R_1, R_2, R_3 and R_4 sets of partons. For comparison we also show the MRS(A') [24] and GRV [9] gluons for $x < 10^{-3}$ at $Q^2 = 5 \text{ GeV}^2$.
- Fig. 6 The next-to-leading-order QCD description of the CDF [7] and D0 [8] single jet inclusive E_T distribution by the R_1 and R_2 sets of partons. These data are not included in the global analysis. The overall normalization of the QCD predictions is fitted to the data sets and the value found in each case is shown on the individual plots.

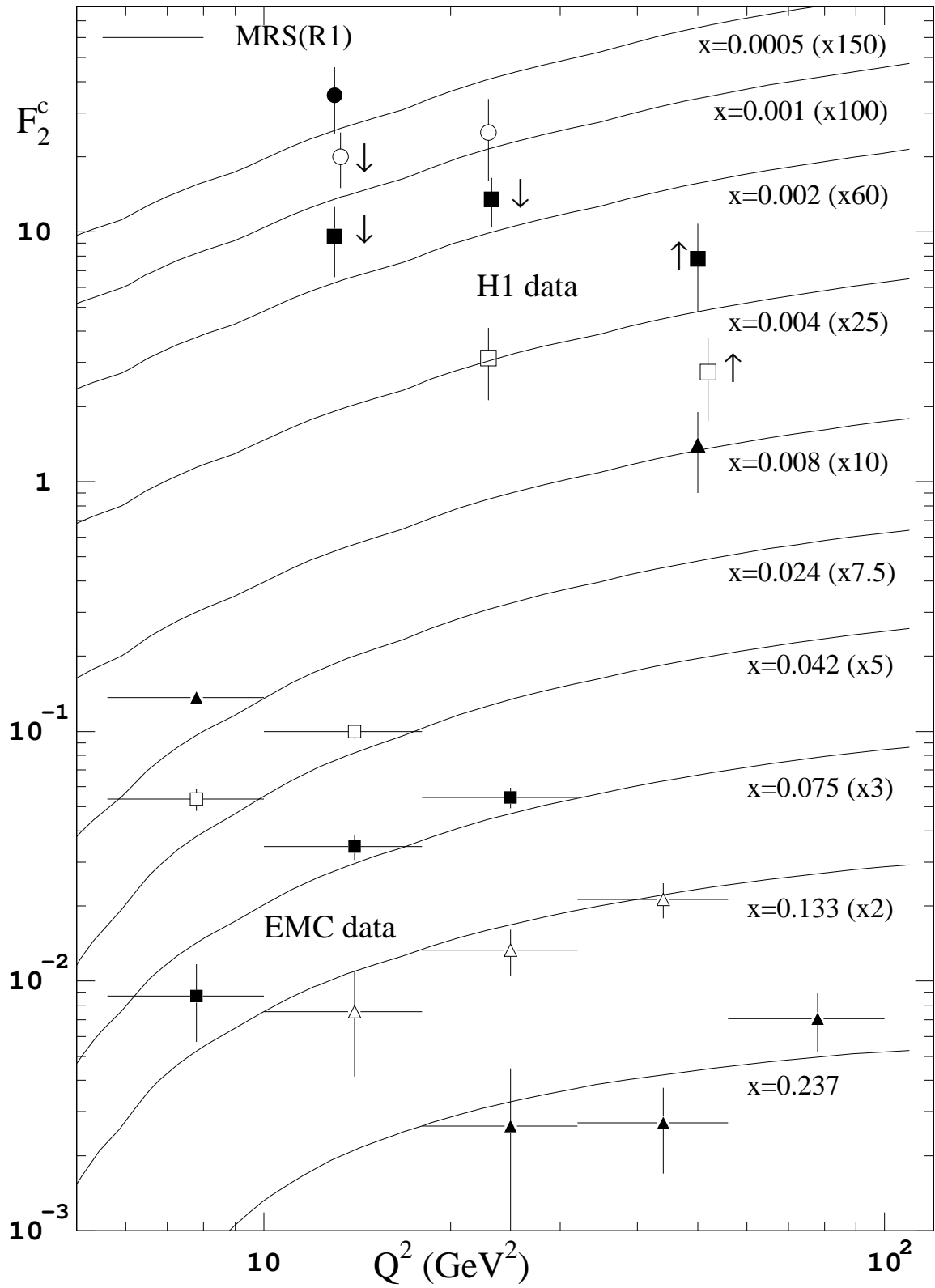


Fig. 1

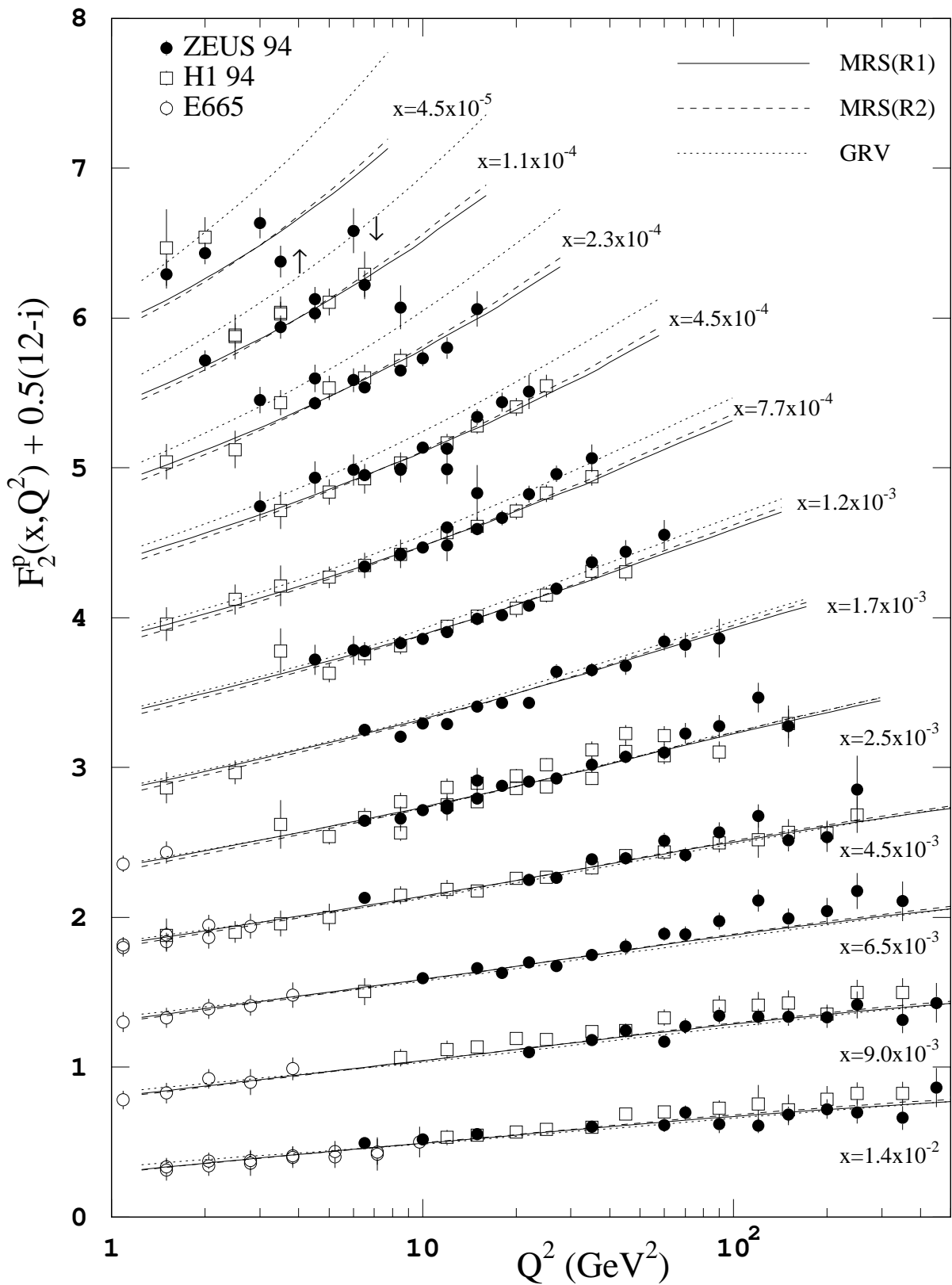


Fig. 2

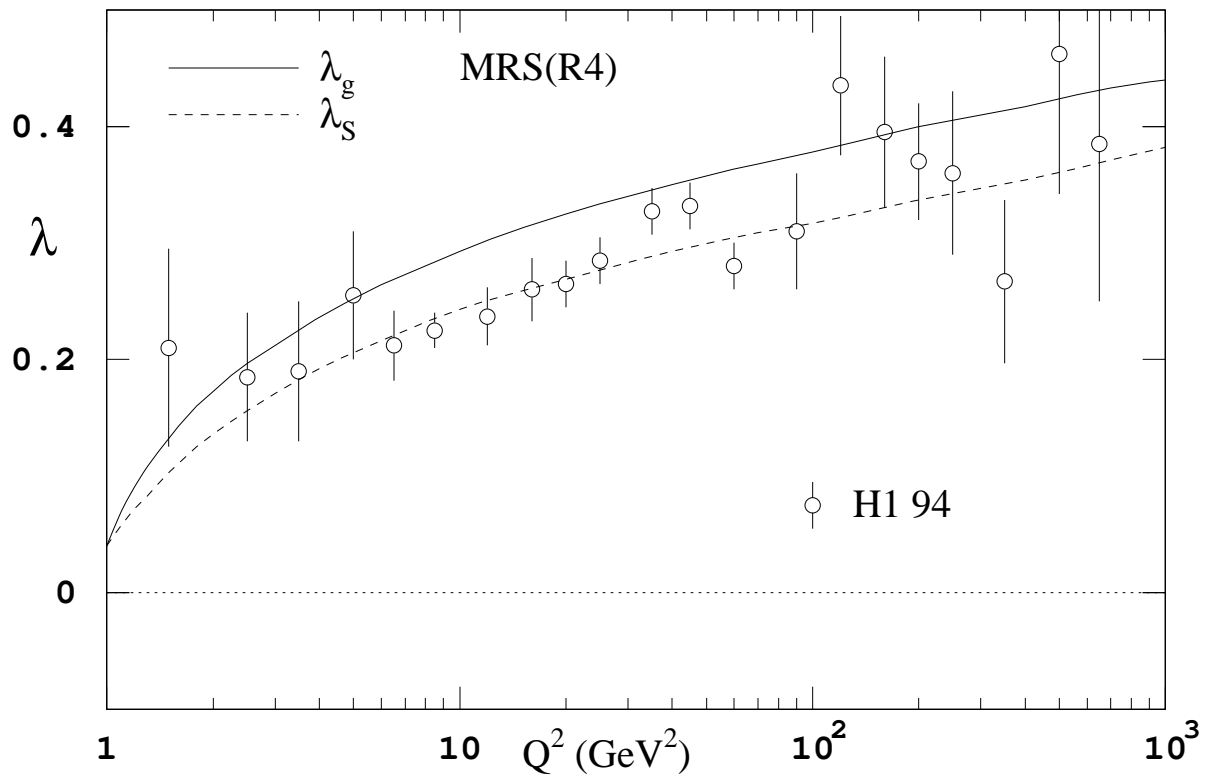
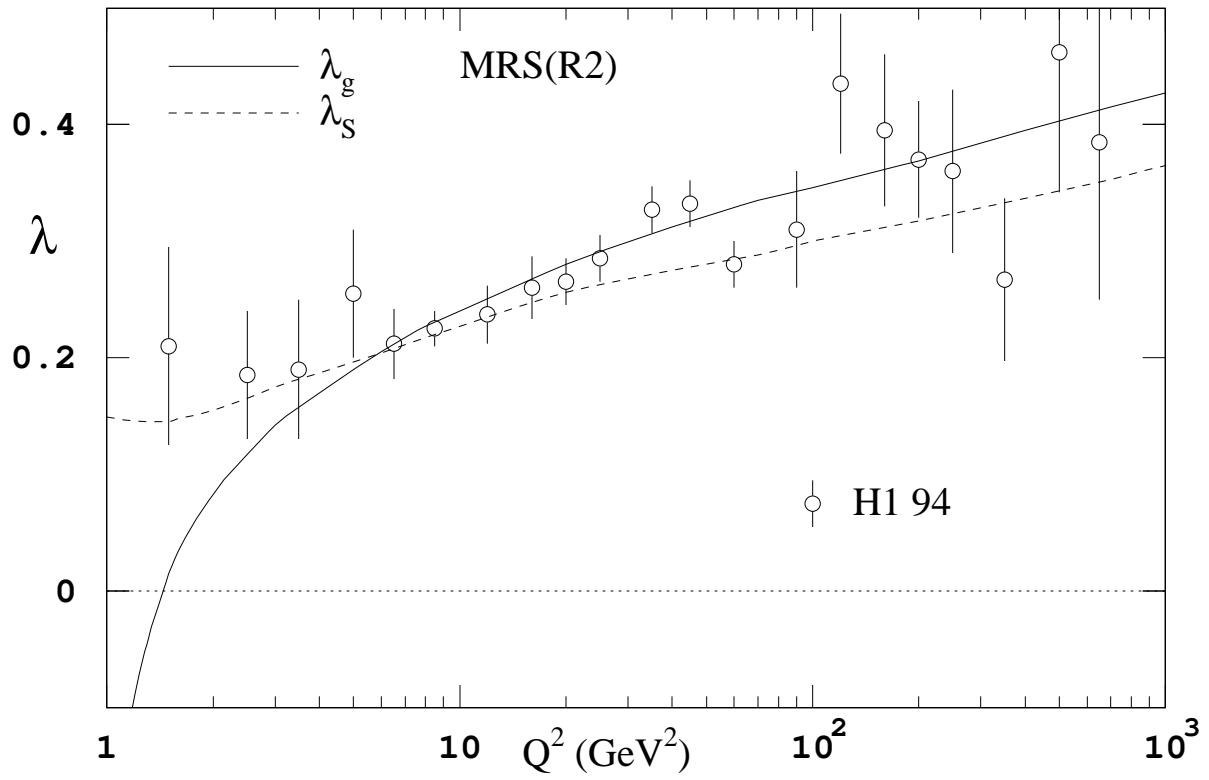


Fig. 3

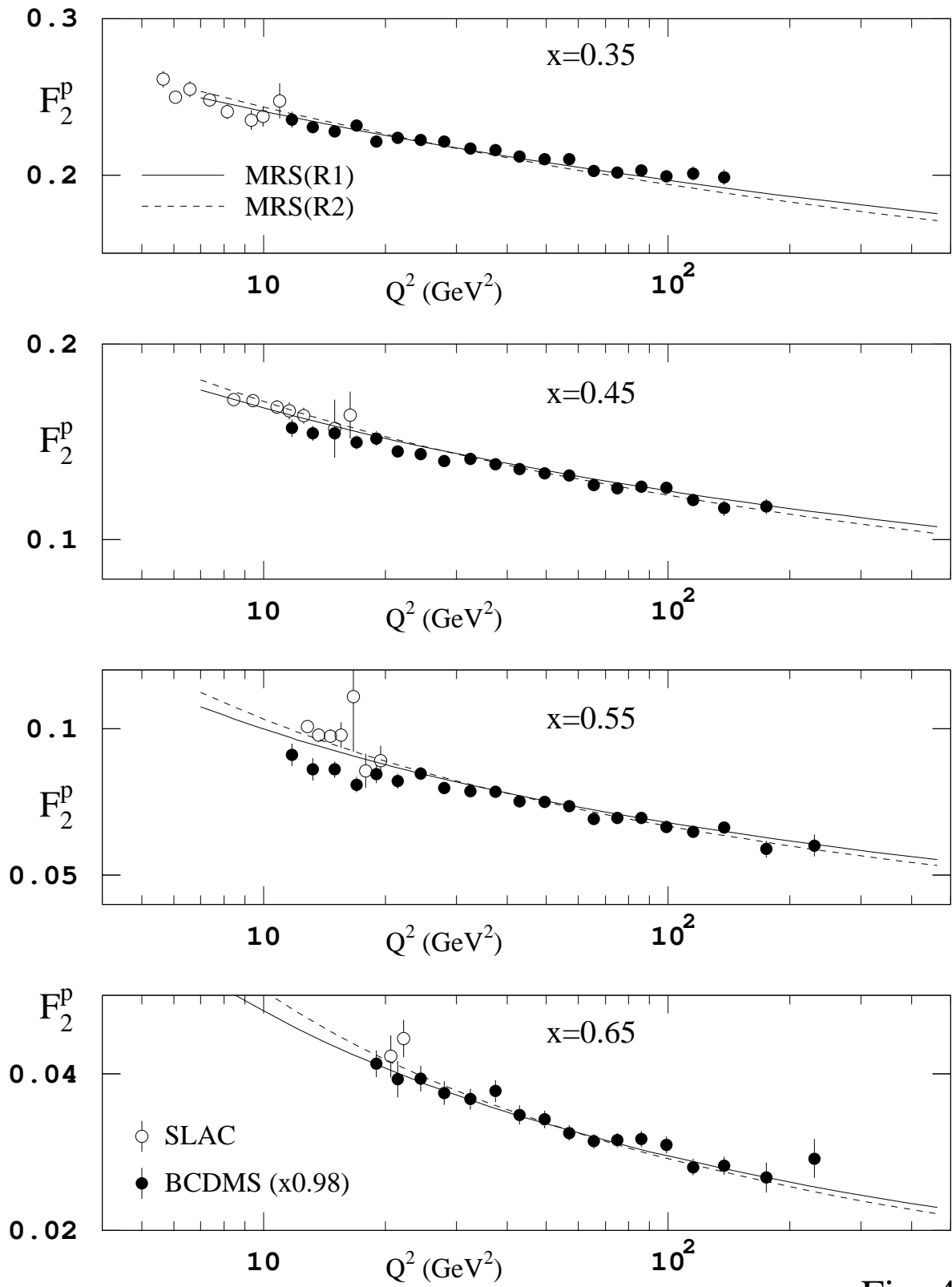


Fig. 4

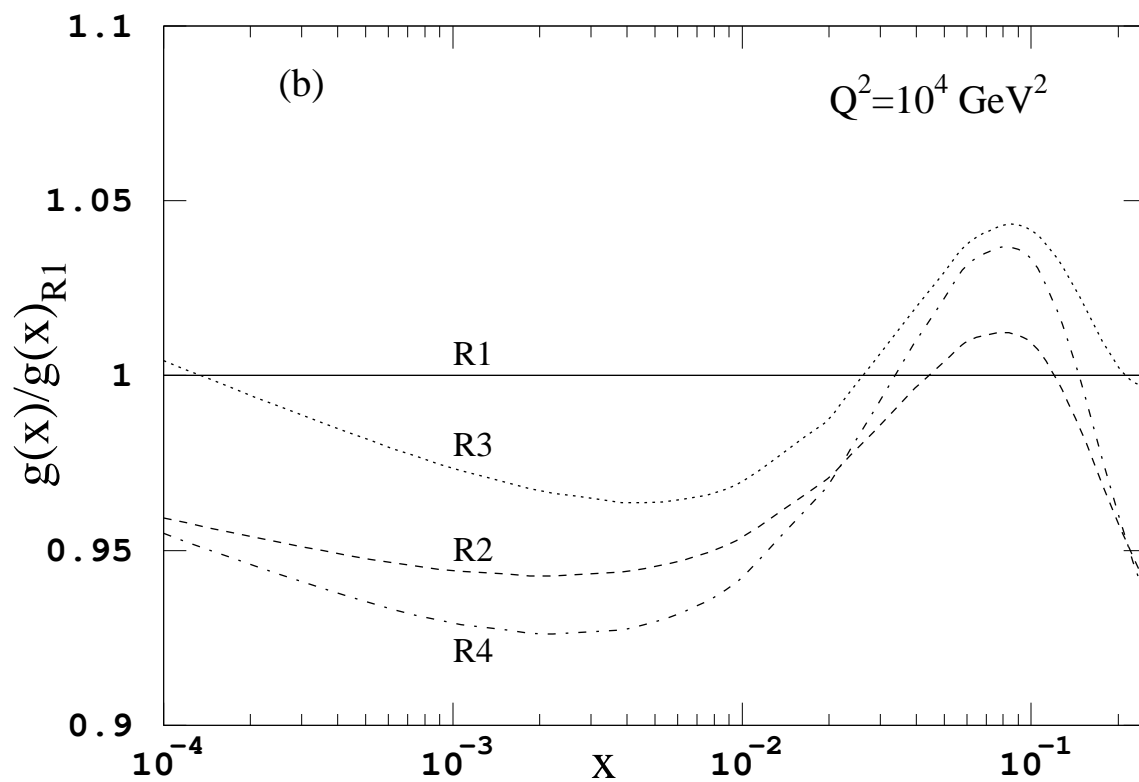
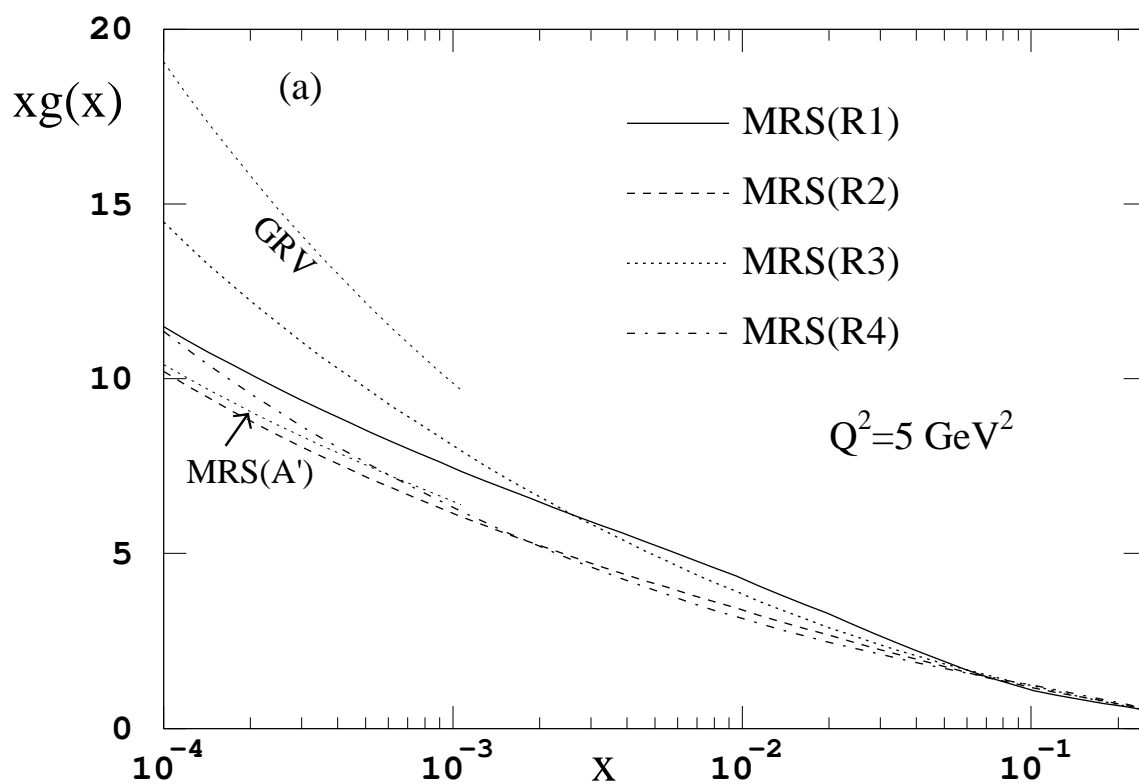


Fig. 5

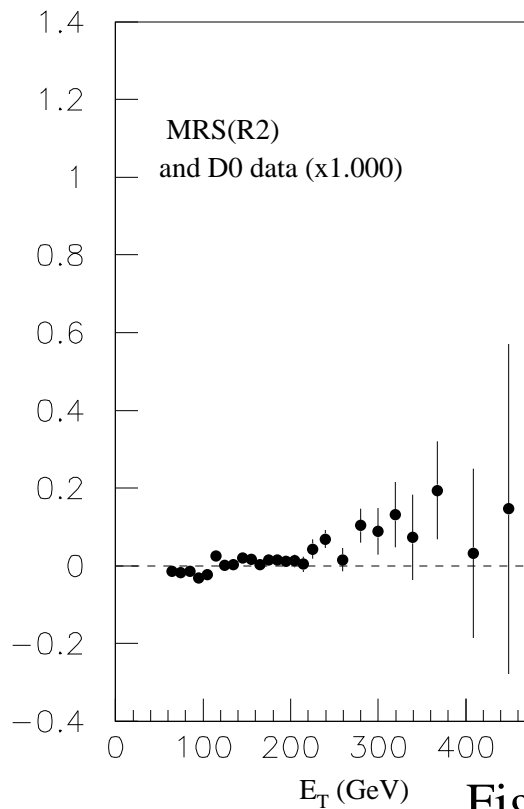
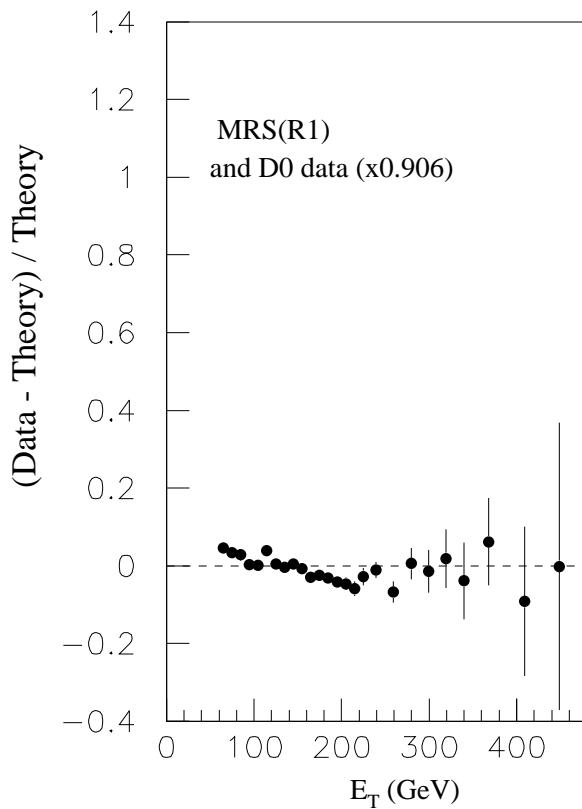
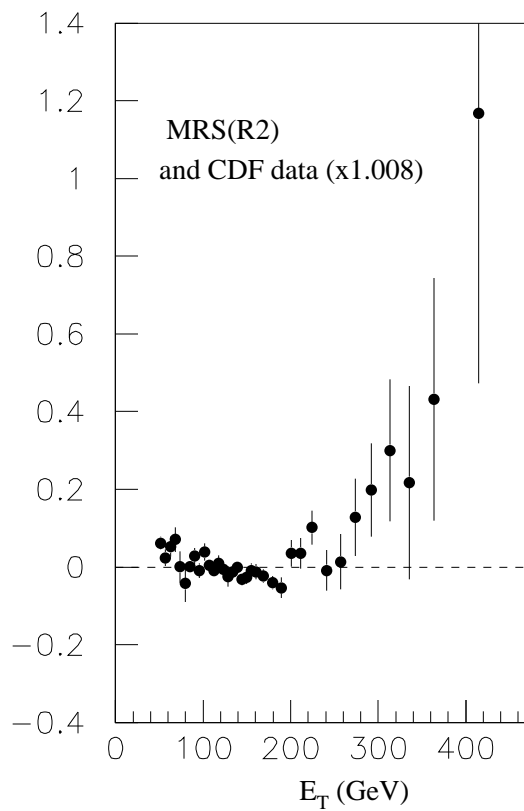
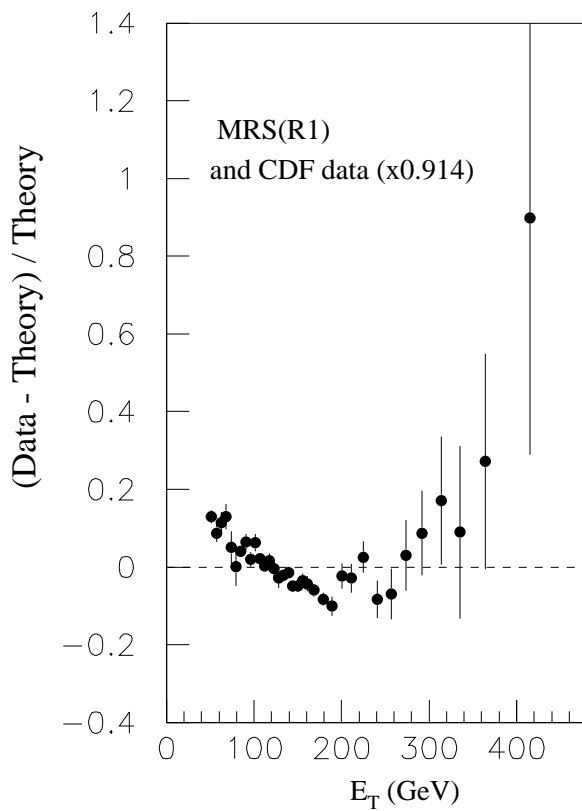


Fig. 6